Early-Age Autogenous Shrinkage and Cracking Risk of 5D Hooked-End Steel Fiber–Reinforced High-Strength Concrete under Uniaxial Restrained Condition

Jiacheng Kang[1]; Dejian Shen[2]; Ci Liu[3]; Ming Li[4]; Chuyuan Wen[5]; and Xiang Shi[6]

Abstract: The incorporation of steel fiber exhibits great benefits to reduce cracking risk and autogenous shrinkage (AS) of high-strength concrete (HSC). 5D hooked-end steel fiber (5DSF) is a kind of novel hooked-end steel fiber. Previous investigations mainly focused on the mechanical properties and shrinkage deformation of 5DSF reinforced HSC (5DSFRC). However, the early-age cracking risk of 5DSFRC under uniaxial restrained conditions considering temperature evolution, AS, and restrained stress simultaneously has not been thoroughly investigated. A temperature stress test machine, which is capable of measuring these factors simultaneously, was used to investigate the effect of 5DSF volume fraction (0%, 0.12%, 0.24%, and 0.36%) on the early-age cracking risk of HSC in the present study. Experimental results and analysis showed that the cracking age, cracking stress, ratio of cracking stress to axial tensile strength, and reserve strength of HSC increased with an increase in 5DSF volume fraction. The AS of HSC decreased with an increase in 5DSF volume fraction, and an AS formula was proposed to calculate the early-age AS of HSC reinforced with steel fiber considering the effect of the volume fraction and shape of the fiber. The cracking risk of HSC decreased with an increase in 5DSF volume fraction. The early-age cracking risk and AS of HSC reinforced with 5DSF were lower than that of HSC reinforced with 3D hooked-end steel fiber with a similar steel fiber volume fraction. **DOI: 10.1061/JMCEE7.MTENG-15446.** © *2023 American Society of Civil Engineers.*

Author keywords: High-strength concrete (HSC); Early age; Cracking risk; Autogenous shrinkage (AS); Hooked-end steel fiber.

Introduction

High-strength concrete (HSC) has been used in many structures due to its excellent mechanical and durability characteristics. However, the low water–cement ratio of HSC results in great self-desiccation (Weiss et al. 1998). The change in the capillary pressure induced by self-desiccation is the driving force of autogenous shrinkage (AS) (Kang et al. 2022; Tang et al. 2021). Tensile stress develops in HSC members when the HSC member is under restrained conditions (Maruyama and Lura 2019; Shen et al. 2022b), and if the tensile stress exceeds the tensile strength of the HSC, it results in the development of cracks (Shah and Weiss 2006). The cracks would offer access to destructive substances containing moisture and aggressive chemical ions (Nili and Afroughsabet 2012), which may compromise the integrity, durability, and service life of concrete structures (Şahmaran et al. 2013; Shen et al. 2022a). Early age is one of the most critical periods of the lifetime of concrete, and AS develops quickly in this period (Shen et al. 2020; Voigt et al. 2005). Hence, investigations on the methods to reduce the AS and cracking risk of HSC at early age considering economy and effectiveness simultaneously are necessary.

Incorporation of fibers exhibits great benefits to reduce cracking risk and AS of HSC (Gholampour and Ozbakkaloglu 2018). The early-age cracking risk refers to the probability of the formation of cracks in the concrete at early age. Nowadays, concrete composites reinforced with advanced fibers such as basalt fiber (Li et al. 2022), glass fiber (Guzlena and Sakale 2021), carbon fiber (Liu et al. 2020), polymer fiber (Chen et al. 2020), and steel fiber (Abdallah et al. 2016; De Smedt et al. 2020) are widely used in the construction industry. Steel fiber is the most widely used one among various kinds of fibers, and is the most adequate fiber for concrete due to its advanced and economical manufacturing facilities, reinforcing effect, and ability to cope with changing environmental conditions (Afroughsabet et al. 2016; Kalpana and Tayu 2020). Steel fiber–reinforced HSC (SFRC) has been used in construction widely over the last few decades (Venkateshwaran et al. 2018). Steel fiber can be categorized into straight, crimped, spiral, twisted, and hooked-end steel fiber according to geometric shape (Abdallah et al. 2017). A statistical analysis of the assortment depicts that more than half

[1]Research Student, College of Civil and Transportation Engineering, Hohai Univ., No. 1, Xikang Rd., Nanjing 210098, China; Research Student, Jiangsu Engineering Research Center of Crack Control in Concrete, No. 1, Xikang Rd., Nanjing 210098, China. Email: kangjiachenghhu@hhu.edu.cn

[2]Professor, College of Civil and Transportation Engineering, Hohai Univ., No. 1, Xikang Rd., Nanjing 210098, China; Deputy Director, Jiangsu Engineering Research Center of Crack Control in Concrete, No. 1, Xikang Rd., Nanjing 210098, China (corresponding author). ORCID: https://orcid.org/0000-0002-0283-6835. Email: shendjn@163.com

[3]Research Student, College of Civil and Transportation Engineering, Hohai Univ., No. 1, Xikang Rd., Nanjing 210098, China; Research Student, Jiangsu Engineering Research Center of Crack Control in Concrete, No. 1, Xikang Rd., Nanjing 210098, China. Email: cliu1995@163.com

[4]Research Student, College of Civil and Transportation Engineering, Hohai Univ., No. 1, Xikang Rd., Nanjing 210098, China; Research Student, Jiangsu Engineering Research Center of Crack Control in Concrete, No. 1, Xikang Rd., Nanjing 210098, China. Email: lim@hhu.edu.cn

[5]Research Student, College of Civil and Transportation Engineering, Hohai Univ., No. 1, Xikang Rd., Nanjing 210098, China; Research Student, Jiangsu Engineering Research Center of Crack Control in Concrete, No. 1, Xikang Rd., Nanjing 210098, China. Email: wenchuyuan_hhu@163.com

[6]Research Student, College of Civil and Transportation Engineering, Hohai Univ., No. 1, Xikang Rd., Nanjing 210098, China; Research Student, Jiangsu Engineering Research Center of Crack Control in Concrete, No. 1, Xikang Rd., Nanjing 210098, China. Email: shixianghhu@163.com

Note. This manuscript was submitted on August 23, 2022; approved on December 9, 2022; published online on May 16, 2023. Discussion period open until October 16, 2023; separate discussions must be submitted for individual papers. This paper is part of the ***Journal of Materials in Civil Engineering***, © ASCE, ISSN 0899-1561.

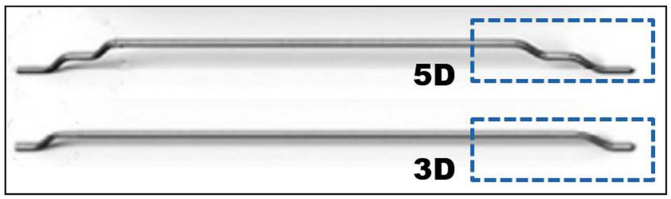

Fig. 1. The geometry of 5D hooked-end and 3D hooked-end steel fiber.

of sold fibers are hooked-end steel fibers (Pająk and Ponikiewski 2013). 5D hooked-end steel fiber (5DSF) is a kind of novel hooked-end steel fiber, which has a higher level of fiber anchoring, tensile strength, and ductility than traditional 3D hooked-end steel fiber (3DSF) (Dehghani and Aslani 2021). The 5DSFs and 3DSFs are different in geometry, as depicted in Fig. 1. A considerable amount of studies have been conducted on the effects of 5DSF on different properties, such as mechanical properties (Afroughsabet et al. 2017; Lee et al. 2019; Murugan et al. 2020), shrinkage deformation (Al-Naimi and Abbas 2021), pull-out strength (Abdallah et al. 2018; De Smedt 2018), peak and postpeak strength (Abdallah et al. 2018), and so on. Although many studies in the field of 5DSFRC only focus on postcracking behavior because the main effect of steel fiber is to bridge the cracks and transfer stress across the cracks after the initial cracking in concrete, the evaluation of precracking behavior of SFRC at early age is equally important (Afroughsabet et al. 2016). Shen et al. (2019c) investigated the early-age cracking risk of 3DSF reinforced HSC (3DSFRC). However, there has been little quantitative analysis of the precracking behavior of 5DSFRC. Hence, investigations on early-age cracking risk of 5DSFRC considering AS are necessary to better understand the cracking mechanisms of SFRC.

The specific objective of this study was to investigate the early-age AS and cracking risk of 5DSFRC under uniaxial restrained conditions. To achieve this, the effect of different steel fiber volume fractions on temperature evolution, AS, and restrained stress of the HSC was tested using temperature stress test machine (TSTM). Experimental results provided fundamental information for the application of 5DSF. An AS formula was proposed to calculate the early-age AS of SFRC considering the effect of volume fraction and shape of the fiber.

Experimental Program

Materials

Portland cement of 52.5R grades with a specific surface area of 375 m^2/kg was used in accordance with GB175 (Chinese Standard 2018) and ASTM C150 (ASTM 2020). The chemical compositions and compressive strength of the portland cement are depicted in Table 1. Crushed limestone with a maximum aggregate size of 25 mm, and natural river sand with a fineness modulus of 2.25 were used in the mixture. The 5DSF with a length of 60 mm and a diameter of 0.75 mm was used, as depicted in Table 2. A kind of liquid polycarboxylate-based superplasticizer was used to ensure adequate workability.

Mixture Proportions and Mixing Process

The mixture proportions of concrete are depicted in Table 3. The mixtures SF00, 5DSF12, 5DSF24, and 5DSF36 with a water–cement ratio of 0.32 were prepared with 5DSF volume fractions of 0%, 0.12%, 0.24%, and 0.36%, respectively. 5DSF was used to substitute coarse aggregate partly by volume, as reported by Nataraja et al. (1999). The mixture SF00 without 5DSF was set as the reference concrete. The same raw materials were used in four mixtures. The dry aggregates were mixed with cement for 1 min, then half of the superplasticizer and water were added and mixed for another 2 min. Then 5DSFs were slowly sprinkled into the mixer and mixed for 1 min. Finally, the remaining superplasticizer and water were added and mixed for 1 min.

Table 1. The chemical compositions and compressive strength of portland cement

Item	Portland cement
SiO_2	19.9%
Al_2O_3	4.6%
Fe_2O_3	3.0%
CaO	64.6%
MgO	0.78%
SO_3	2.37%
Na_2O	0.06%
K_2O	0.65%
Cl^-	0.01%
3-day compressive strength	35.6 MPa
28-day compressive strength	66.9 MPa

Table 2. Mechanical and chemical properties of steel fiber

Properties	5DSF
Diameter	0.75 mm
Length	60.0 mm
Axial tensile strength	1,225 MPa
Elastic modulus	200 GPa
Hooked-length	4 mm
Hooked-angle	45°
C	≤0.90%
Si	≤0.40%
Mn	≤1.00%
P	≤0.020%
S	≤0.010%

Table 3. Mixture proportions and slump of concrete composites

Mixture composition	Unit	SF00	5DSF12	5DSF24	5DSF36
Water	kg/m^3	153.6	153.6	153.6	153.6
Cement	kg/m^3	480	480	480	480
Fine aggregate	kg/m^3	690	690	690	690
Coarse aggregate	kg/m^3	1,127.00	1,123.32	1,119.63	1,115.95
Superplasticizer	kg/m^3	3.84	3.84	3.84	3.84
Steel fiber	kg/m^3	0	9.42	18.84	28.26
Steel fiber volume fraction	%	0	0.12	0.24	0.36
Slump	mm	165	153	142	131

TSTM Test

Test Details

TSTM consisted of two aluminum molds, controller, stepper motor, displacement meter, temperature sensor, and load cell, as depicted in Fig. 2. The molds were used for restrained and free shrinkage tests, as reported by Kovler (1994). The stress process, deformation, and temperature evolution of two concrete specimens were

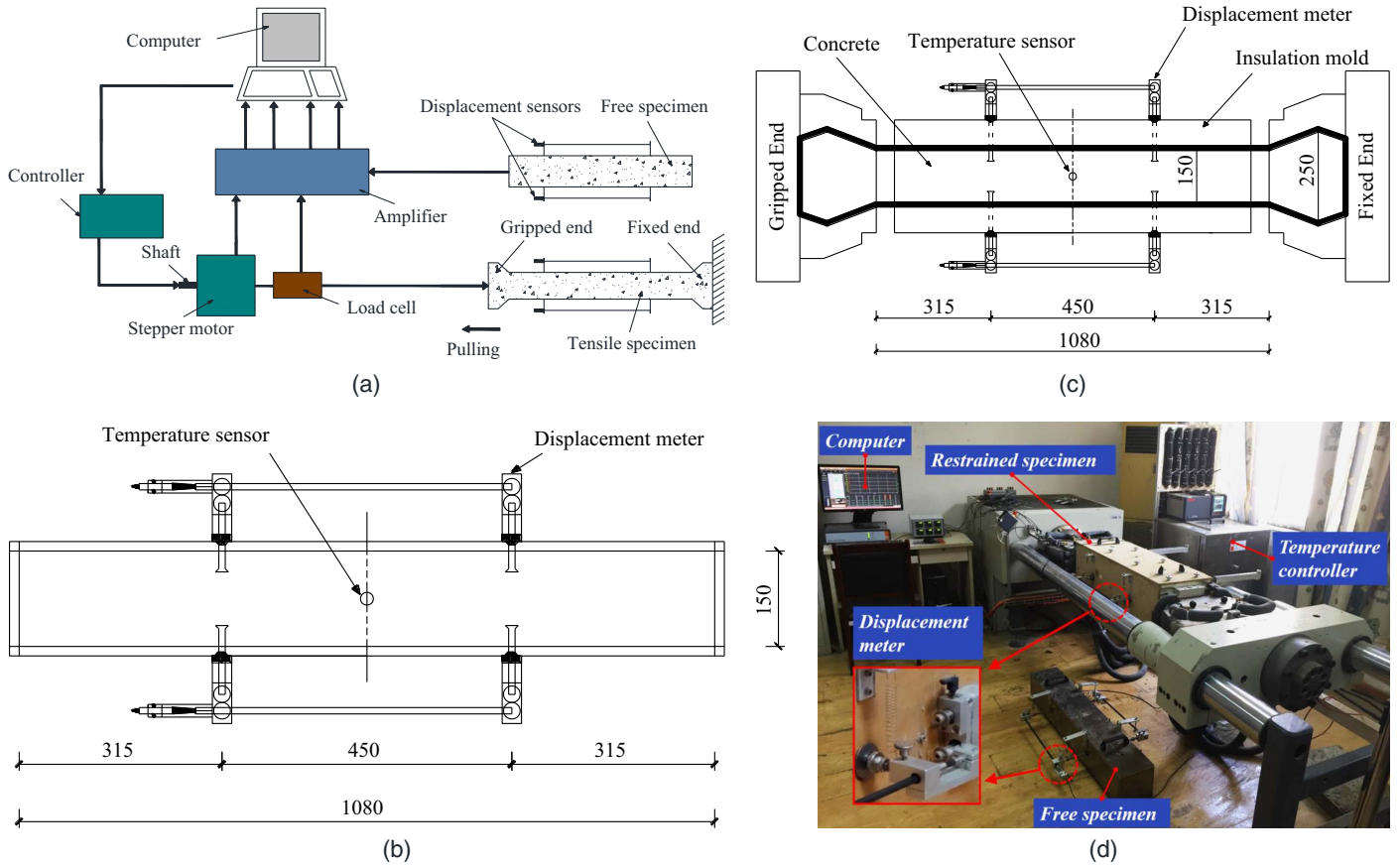

Fig. 2. Schematic description adapted from TSTM: (a) schematic description (adapted from Kovler 1994); (b) dimension of free specimen (mm); (c) dimension of restrained shrinkage specimen (mm); and (d) picture of experiment equipment.

measured by the load cell, displacement meter, and temperature sensor, respectively. TSTM pulls or pushes the gripped end of the restrained shrinkage specimen through a stepper motor to provide the various restraint degrees (Zhang and Qin 2006). The temperature of the concrete specimen was controlled with a mixture of special liquid and water (1:1) circulating along the molds, as reported by Kovler et al. (1999) and Kovler (1994). The circulating liquid is heated and cooled by a temperature controller.

The restrained shrinkage specimen was in a dog-bone shape, and the dimension of the cross section was 150×150 mm in the center part and 150×200 mm at the ends. To reduce the possibility of stress concentration in the concrete specimens, a rounded transition area was set between the center part and the two ends. The free shrinkage specimen was a prism with two free ends, and the dimension of the cross section was 150×150 mm. The displacement meter equipped with two fixing devices was installed on the sides of the molds before casting, and the length between the two fixing devices was 450 mm, as depicted in Fig. 2.

Testing Procedure

Plastic sheets were placed in the two molds before casting to reduce friction, and the top surfaces of the two specimens were sealed immediately after casting to maintain a constant humidity, as reported by Wei and Hansen (2013). The temperature sensor was inserted in the central part of the concrete specimen directly after casting. Concrete specimens were cured and tested under the same curing condition. The two concrete specimens were covered around by the temperature-regulation molds, which included circulating fluid flowing in the pipes, to ensure the uniform temperature distribution over the cross section and to ensure the two concrete specimens had the same temperature history. The restrained shrinkage specimens were cured under adiabatic temperature rise mode, as recommended by Zhao et al. (2019). The adiabatic temperature rise mode is a semiadiabatic condition due to the loss of temperature to the surroundings. The concrete specimens maintained peak temperature for 36 h, and then cooled down at the rate of 2°C/h until cracking. The cooling rate of 2°C/h is reasonable, which could minimize the viscoelastic influence and prevent the formation of large thermal gradients (Schlitter et al. 2013). The restrained shrinkage specimen under full restrained condition was pulled or pushed to its original position when the strain of the restrained shrinkage specimens reached 2.0 $\mu\varepsilon$, as reported by Zhang and Qin (2006). The results of temperature, restrained stress, and deformation of the specimen were automatically recorded by a computer every 5 min.

Experimental Results and Discussion

Effect of 5D Hooked-End Steel Fiber on Temperature Evolution

Early-age cracking risk of concrete is affected by its temperature evolution. Several factors, such as the composition and content of cement, the casting and curing condition of the concrete, and the mixture proportion, are known to affect the temperature evolution of concrete. Eq. (1) is used to calculate the adiabatic temperature

J. Mater. Civ. Eng., 2023, 35(8): 04023220

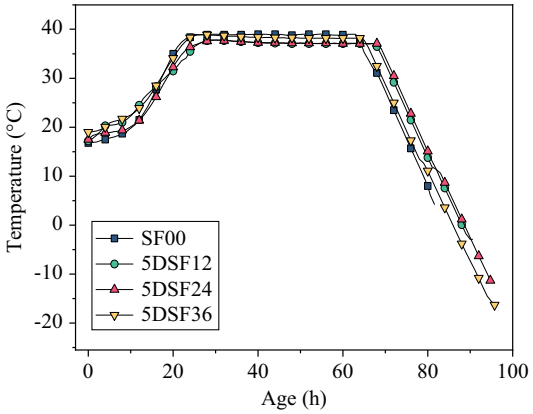

Fig. 3. Temperature evolution of restrained shrinkage specimen for four concrete mixtures.

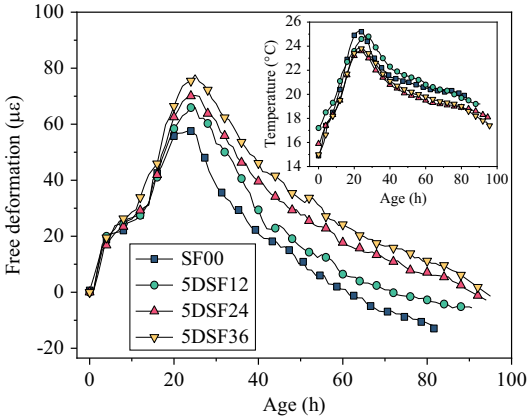

Fig. 4. Total deformation and temperature evolution of free specimen for four concrete mixtures.

rise, which is the differential value between peak temperature T_{ht} and casting temperature T_{ct} (Shen et al. 2018a)

$$T_{tr} = T_{ht} - T_{ct} \tag{1}$$

where T_{tr} is the adiabatic temperature rise, in °C; T_{ht} is the peak temperature, in °C; and T_{ct} is the casting temperature, in °C.

Fig. 3 depicts the temperature evolution of the restrained shrinkage specimen for the four concrete mixtures. Results reveal that the temperature rise for the four mixtures were 22.2°C, 20.6°C, 20.3°C, and 19.9°C, which decreased by 7.21%, 8.56%, and 10.36% with an increase in 5DSF volume fraction ranging from 0% to 0.12%, 0.24%, and 0.36%, respectively. The results of adiabatic temperature rise are similar to the data obtained by Shen et al. (2017). This result may be explained by the fact that the adiabatic temperature rise is mainly affected by the quality and dosage of cement, and the water in the concrete. 5DSF does not participate in cement hydration, and the quantity of cement and water used in the present study were the same for all four mixtures. Also, the thermal conductivity of HSC increases by incorporating 5DSF (Li et al. 2021). Hence, the heat in the center of the HSC spread to the surroundings more easily, and the adiabatic temperature rise for all four mixtures was slightly lower with an increase in 5DSF volume fraction.

Considering that the temperature of the free specimen was not constant, Eq. (2) is used to convert the actual age of the free specimen to the equivalent age at 20°C (Krauß et al. 2001)

$$t_e = \int_0^t \exp\left[\frac{E_a(T)}{R}\left(\frac{1}{T_{ref}+273} - \frac{1}{T(t)+273}\right)\right]dt \tag{2}$$

where t_e is the equivalent age at 20°C, in h; $T(t)$ is the actual temperature, in °C, in h; R is the ideal gas constant (8.315 J/mol/K); T_{ref} is a reference temperature (20°C); and $E_a(T)$ is the activation energy, in kJ/mol [$T(t) \geq 20$°C, $E_a(T) = 33.5$ kJ/mol; $T(t) < 20$°C, $E_a(T) = 33.5 + 1.47(20 - T(t))$ kJ/mol].

The equivalent age of concrete is determined in the discrete form with Eq. (3) (Krauß et al. 2001)

$$t_e = \sum \exp\left[\frac{E_a(T)}{R}\left(\frac{1}{T_{ref}+273} - \frac{1}{T(t)+273}\right)\right]\Delta t \tag{3}$$

Effect of 5D Hooked-End Steel Fiber on Autogenous Shrinkage

The deformation of concrete is complicated, especially in the first few hours after casting (Shen et al. 2018b). Generally, the deformation of concrete fails to be measured immediately after casting. The time-zero is determined as the starting point of AS, and various methods are used to define time-zero (Huang and Ye 2017; Lura et al. 2001; Meddah et al. 2006; Meddah and Tagnit-Hamou 2011; Miao et al. 2007; Tenório Filho et al. 2019). Only stress-induced deformations were investigated in the present study, hence, time-zero was defined as the first moment when stress was recorded, and the value of AS was set to be zero a time-zero in the TSTM test, as reported by Lura et al. (2001).

The macroscopic bulk deformation of concrete under a sealed and isothermal condition is defined as AS (De la Varga et al. 2012), which develops mostly at early age because the internal humidity drops rapidly at this stage, and the capillary pressure increases during this phase (Aly and Sanjayan 2008; Şahmaran et al. 2009). In the present study, total deformation and temperature evolution of the free specimen were measured by a displacement meter and a temperature sensor, respectively, as depicted in Fig. 4 and recommended by Igarashi et al. (2000). The deformations measured in the free specimen mainly consist of AS and thermal deformation, as given in Eq. (4), and the thermal deformation caused by temperature change can be obtained with Eq. (5) (Chu et al. 2012; Shi et al. 2014)

$$\varepsilon_{total} = \varepsilon_{as} + \varepsilon_T \tag{4}$$

$$\varepsilon_T = \alpha \times \Delta T \tag{5}$$

where ε_{total} is the total deformation, in $\mu\varepsilon$; ε_{as} is the AS deformation, in $\mu\varepsilon$; ε_T is the thermal deformation, in $\mu\varepsilon$; α is the coefficient of thermal expansion (CTE), in $\mu\varepsilon$/°C; and ΔT is the temperature change, in °C.

AS is the volume change of concrete under constant temperature (De la Varga et al. 2012), while the curing mode was adiabatic temperature rise mode, and the temperature of concrete was changing with age due to the development of cement hydration. Hence, the thermal deformation must be separated from total deformation to obtain the AS. There are two ways of separating AS according to previous studies (Chu et al. 2012; Turcry et al. 2002): the one way is based on the maturity theory, which deduces the AS of concrete with varying temperatures by measuring the AS at a constant temperature of 20°C; the other way is based on the value of CTE determined by existing models or directly assumed as a constant between 8 and 12 $\mu\varepsilon$/°C, and combined with the temperature evolution of the concrete to obtain the thermal deformation of the concrete, and then finally separate it from total deformation to obtain

the AS. In the present study, the second method was adopted to determine the AS. The CTE of concrete changed greatly, and the AS developed rapidly within one day after casting. The CTE of concrete is large immediately after casting, but decreases rapidly and then gradually becomes stable (Viviani et al. 2007). In the early stage after casting, the concrete contained a great amount of free water, the CTE of which was larger than that of the solid in the concrete. Hence, the CTE of concrete was large initially after casting. The CTE of concrete gradually decreased and became stable due to the completion of cement hydration (Zhu et al. 2022a, b). The 28-day CTE of concrete was determined as 7 $\mu\varepsilon/$℃ in the present study, and the CTE varying with age was calculated by a simplified prediction model proposed by Zhang et al. (2010), as given in Eq. (6)

$$\alpha_T(t) = \alpha_k \cdot (1 + 41 \cdot t^{-m}) \tag{6}$$

where $\alpha_T(t)$ *is* the concrete CTE at t d, in $\mu\varepsilon/$℃; α_k is the 28-day concrete CTE, in $\mu\varepsilon/$℃; t is the actual age of concrete after casting, in h; and m is 2.0.

AS is calculated by subtracting thermal deformation from total deformation with Eq. (7), as reported by Chu et al. (2012)

$$\varepsilon_{as}(t) = \varepsilon_{total} - \alpha_T(t) \times [T(t) - T_{time-zero}] \tag{7}$$

where $\varepsilon_{as}(t)$ is the AS deformation at t days, in $\mu\varepsilon$; $T(t)$ is the temperature at t days, in ℃; and $T_{time-zero}$ is the time-zero temperature of HSC, in ℃. AS of the free specimen for the four mixtures are depicted in Fig. 5.

During the process of concrete hardening, a solid mesh of capillary pores filled with water was formed. The amount of water in capillary pores reduced during the process of cement hydration (Shen et al. 2022c), and then the capillary pressure increased, which resulted in the increase of AS deformation with time. The results of AS were calculated with Eq. (7) based on the results of temperature history and deformation obtained from the free shrinkage specimen, as depicted in Fig. 5, which shows that the development rate of AS decreased significantly with an increase in 5DSF volume fraction. The concrete specimen of mixture SF00 cracked first, and the results of AS at the cracking age of SF00 were −128, −97, −82, and −61 $\mu\varepsilon$ for mixtures SF00, SF12, 5DSF24, and 5DSF36, respectively, the absolute value of which decreased by 24.22%, 35.94%, and 52.34% with an increase in 5DSF volume fraction ranging from 0% to 0.12%, 0.24%, and 0.36%, respectively. The results are consistent with data obtained by Bandelj et al. (2011) and Saje et al. (2012). To compare the effect of different 5DSF volume fractions on the AS of concrete, test results were interpreted by one-way ANOVA. The results of one-way ANOVA analysis show that the effect of 5DSF volume fractions on the AS reduction was significant ($p < 0.05$). The measurements suggest that the absolute value of mean AS of concrete decreased by 18.45%, 34.95%, and 51.46% with an increase in 5DSF volume fraction ranging from 0% to 0.12%, 0.24%, and 0.36%, respectively. The decreased mean AS can result in smaller volume change and reduce the cracking risk. Fig. 6 depicts the decreased degree of early-age AS with an increase in volume fractions of steel fibers in different shapes in studies (Bandelj et al. 2011; Meng and Khayat 2018; Shen et al. 2019c; Zheng et al. 2019), and the results revealed that the hooked-end steel fiber showed a higher decrease degree in early-age AS than other steel fibers in different shapes when the steel fiber volume fraction was similar. For instance, Shen et al. (2019c) revealed that when 3DSF was incorporated to HSC, the absolute value of AS decreased by 48.06% when the 3DSF volume fraction increased from 0% to 0.6%. In the present study, when the 5DSF volume fraction increased from 0% to 0.36%, the absolute value of AS decreased by 52.34%. Results indicate that 5DSF is better at inhibiting AS than 3DSF, and the amount of 5DSF needed to achieve a similar effect is less than that of 3DSF. The main reason is that the strength of the bond between matrix and 5DSF is higher than that of 3DSF (De Smedt 2018).

Several explanations may account for the decrease in AS in the present study. First, steel fibers can resist the shrinkage deformation of the HSC effectively because the elastic modulus of concrete at early age is low (Afroughsabet et al. 2016). Second, a water film is formed on the surface of 5DSF during the mixing process, which produces many calcium hydroxide crystals on the surface of 5DSF. Then, a loose reticular structure is formed between 5DSF and matrix, which inhibits the development of AS (Sun et al. 1986). Third, 5DSF can support the skeleton during the process of shrinkage. A range of bond stress distribution is created around the 5DSF close to the cracks due to the tensile stress of fiber, and the development of crack tip will be inhibited due to constraints and barriers of 5DSF (Wu et al. 2017). Hence, the incorporation of 5DSF decreased the AS significantly.

Shen et al. (2019c) proposed an AS formula of 3DSFRC considering the effect of the 3DSF volume fraction. However, the shape of 5DSF is different from that of 3DSF, which would affect

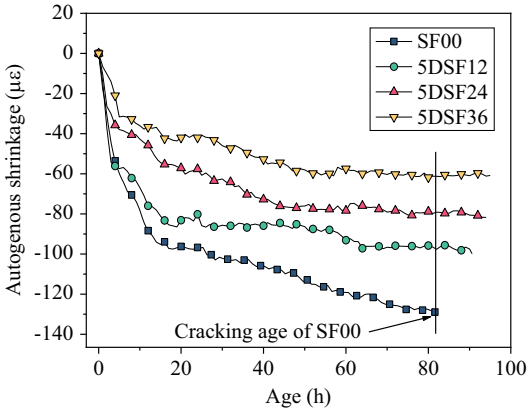

Fig. 5. Autogenous shrinkage of free specimen for four concrete mixtures.

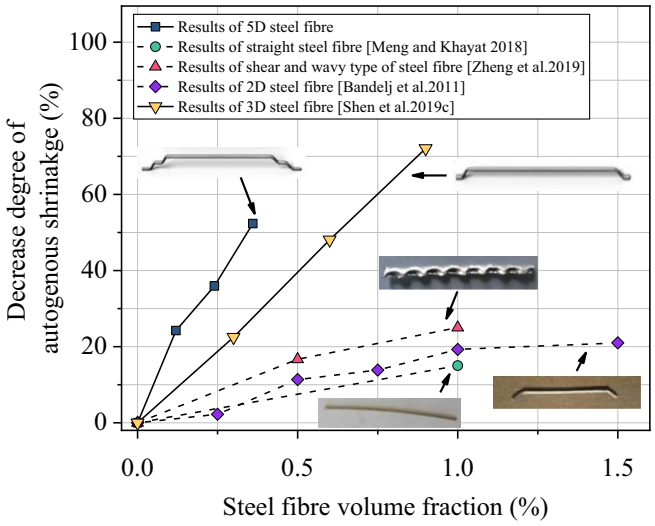

Fig. 6. Decrease degree of early-age autogenous shrinkage with an increase in volume fractions of steel fibers in different shapes.

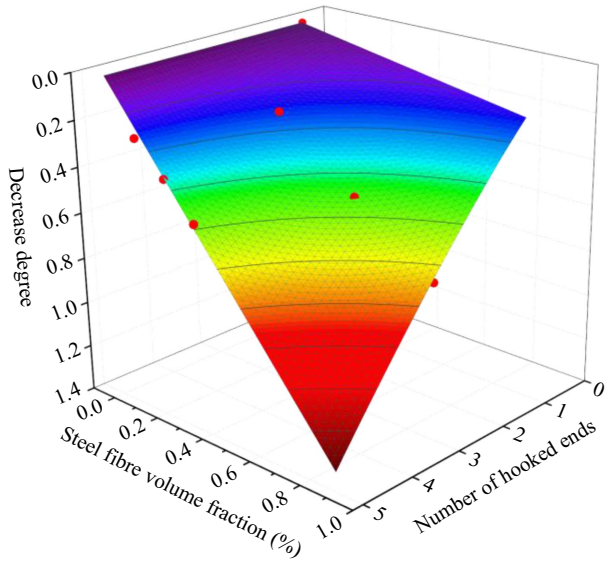

Fig. 7. Influence coefficient of autogenous shrinkage.

the accuracy of the AS formula. Thus, an AS formula considering the volume fractions and shapes of steel fiber is needed. In the present study, an AS formula based on the Tazawa–Miyazawa model (Tazawa and Miyazawa 1995) was proposed to calculate the AS of SFRC reinforced with different volume fractions and shapes of steel fiber, as given in Eq. (8)

$$\begin{aligned} \varepsilon_{cas}(t) &= \varepsilon_{cas0}(\theta, N)\beta_a(t) \\ \varepsilon_{cas0}(\theta, N) &= \varepsilon_{cas0}(0,1) \cdot [1 - f(\theta, N)] \\ \beta_a(t) &= 1 - \mathrm{e}^{(-\mathrm{a}\cdot t^b)} \end{aligned} \tag{8}$$

where $\varepsilon_{cas}(t)$ is the real time-dependent AS, in $\mu\varepsilon$; $\varepsilon_{cas0}(\theta, N)$ is the AS for different mixtures at the cracking age of the reference concrete, in $\mu\varepsilon$; $\varepsilon_{cas0}(0,1)$ is the AS of mixture SF00 at the cracking age (-128 $\mu\varepsilon$), in $\mu\varepsilon$; $f(\theta, N)$ is the influence coefficient of AS considering the content and shape of steel fiber; $\beta_\alpha(t)$ is the development coefficient of AS; and a and b are the fitting parameters.

$f(\theta, N)$ was determined as the reduction in AS compared to the reference concrete for different mixtures [results in the present study and results obtained by Shen et al. (2019c) were included], and the average values of reduction at three ages when AS developed slowly were taken to determine its value (51 h, 62 h, and the cracking age of reference concrete were taken as the three ages for this calculation in the present study) Fig. 7 depicts the results of influence coefficient of AS. Eq. (9) was given to determine the relationship between the influence coefficient of AS and the content, as well as the shape of steel fiber

$$f(\theta, N) = \theta \cdot \left[\frac{\gamma \cdot N}{(l/d)}\right]^{\beta} \tag{9}$$

where l/d is the length–diameter ratio of steel fiber; θ is the steel fiber volume fraction; N is the number of hooked ends; and γ and β is the fitting parameters. The regression results of γ and β were 21.785 and 1.228, and the coefficient of determination (R^2) was 0.983.

The regression results of fitting parameters (a, b) are depicted in Table 4, and the average values of fitting parameters were used in the AS formula. The concrete mixtures of HSC with 3DSF volume fractions of 0.3%, 0.6%, and 0.9% in the study (Shen et al. 2019c) were denoted as 3DSF30, 3DSF60, and 3DSF90, respectively. The AS formula of SFRC reinforced with different volume fractions and shapes of steel fiber is given in Eq. (10). The results of fitting parameters in the AS formula are given in Fig. 8, and the results of AS formula showed that the proposed formula could calculate the AS of concrete reinforced with different volume fractions and shapes of steel fibers effectively

$$\varepsilon_{cas}(t) = \varepsilon_{cas0}(0,1) \cdot \left[1 - \theta \cdot \left[\frac{\gamma \cdot N}{(l/d)}\right]^{\beta}\right]\left[1 - \mathrm{e}^{(-a\cdot t^b)}\right] \tag{10}$$

Effect of 5D Hooked-End Steel Fiber on Restrained Stress

During the hardening phase, the temperature of concrete specimens increased, and the compressive stress developed when the expansion was under uniaxial restrained conditions. Fig. 9 depicts that maximum restrained compressive stress was 0.35, 0.45, 0.57, and 0.64 MPa, which increased by 28.57%, 62.86%, and 82.86% with an increase in 5DSF volume fraction ranging from 0% to 0.12%, 0.24%, and 0.36%, respectively. The results are consistent with data obtained by Shen et al. (2019c). After entering the phase of constant temperature curing, the deformation of concrete specimens was nearly unchanged, and stress relaxation occurred in the concrete specimens due to the low strength as well as elastic modulus, which made the compressive stress decrease gradually, as reported by Mehta and Monteiro (2006).

During the constant temperature curing phase, the compressive stress of mixtures SF00, 5DSF12, 5DSF24, and 5DSF36 decreased gradually to around zero. Fig. 10 depicts the temperature and restrained stress of four mixtures at different ages.

Zero-stress occurs when the restrained compressive stress changes to the restrained tensile one during the cooling phase, and the temperature at the time when zero-stress occurs is defined as zero-stress temperature ($T_{zero-stress}$) (Wei and Hansen 2013). Restrained tensile stress development rate was 1.65, 1.81, 1.87, and 1.93 MPa per day for mixtures SF00, 5DSF12, 5DSF24, and 5DSF36, respectively. During the cooling phase, the stress at the temperature when the concrete is cast is defined as the stress at room temperature, which indicates the stress state of concrete without thermal deformation (Shen et al. 2021). The results of

Table 4. Fitting parameters of autogenous shrinkage for different mixtures in the present study and previous studies

Concrete mixtures	SF00	5DSF12	5DSF24	5DSF36	3DSF30	3DSF60	3DSF90	Average value
a	0.236	0.396	0.179	0.150	0.215	0.246	0.195	0.231
b	0.585	0.414	0.646	0.719	0.650	0.568	0.586	0.595
R^2	0.970	0.941	0.981	0.950	0.984	0.979	0.992	—

Source: Data from Shen et al. (2019c).

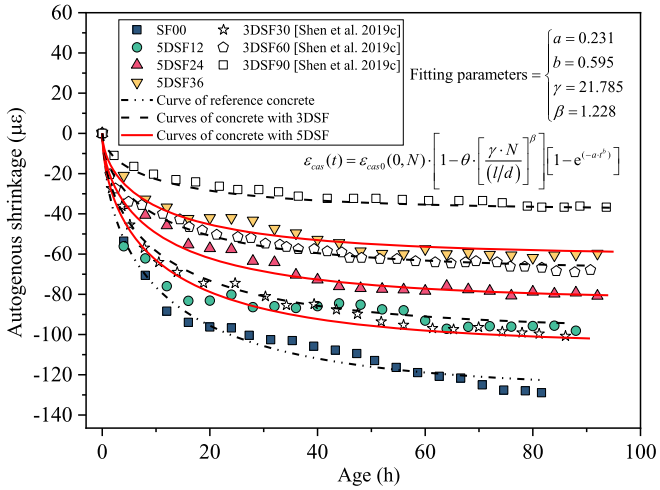

Fig. 8. Autogenous shrinkage formula of HSC reinforced with different volume fractions and shapes of steel fiber.

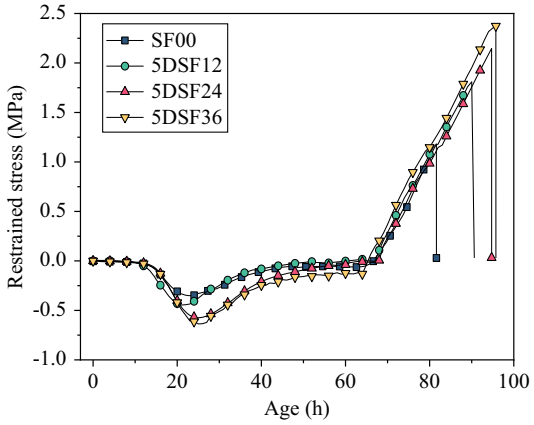

Fig. 9. Restrained stress of four concrete mixtures.

stress at room temperature of 15.8°C, 18.2°C, 17.2°C, and 15.5°C were 0.68, 0.94, 0.92, and 0.83 MPa for mixtures SF00, 5DSF12, 5DSF24, and 5DSF36, respectively. The restrained stress in tension increased when the temperature of the concrete decreased, and cracks occurred when induced stress exceeded the tensile strength of HSC, which was depicted by a sharp drop in Figs. 6 and 7. The cracking stress was 1.18, 1.81, 2.15, and 2.37 MPa at the cracking age of 81.6, 90.6, 94.7, and 95.7 h for mixtures SF00, 5DSF12, 5DSF24, and 5DSF36, and the cracking stress increased by 53.39%, 82.20%, and 100.85% with an increase in 5DSF volume fraction ranging from 0% to 0.12%, 0.24%, and 0.36%, respectively. Results on cracking age and cracking stress of HSC indicated that the incorporation of 5DSF significantly decreased the cracking risk of HSC, as reported by Shen et al. (2019c). A possible explanation for this might be that the restrained shrinkage specimen under full restrained condition was pulled or pushed to its original position when the strain of the restrained shrinkage specimens reached 2.0 $\mu\varepsilon$, and stress was induced in the concrete at early age. The matrix partly transferred the induced stress to the 5DSF before cracks occurred, because the appearance of cracks greatly reduced the ability of concrete to resist further cracking. Hence, the incorporation of 5DSF prevents the growth and development of early-age cracks and significantly decreases the cracking risk (Døssland 2008).

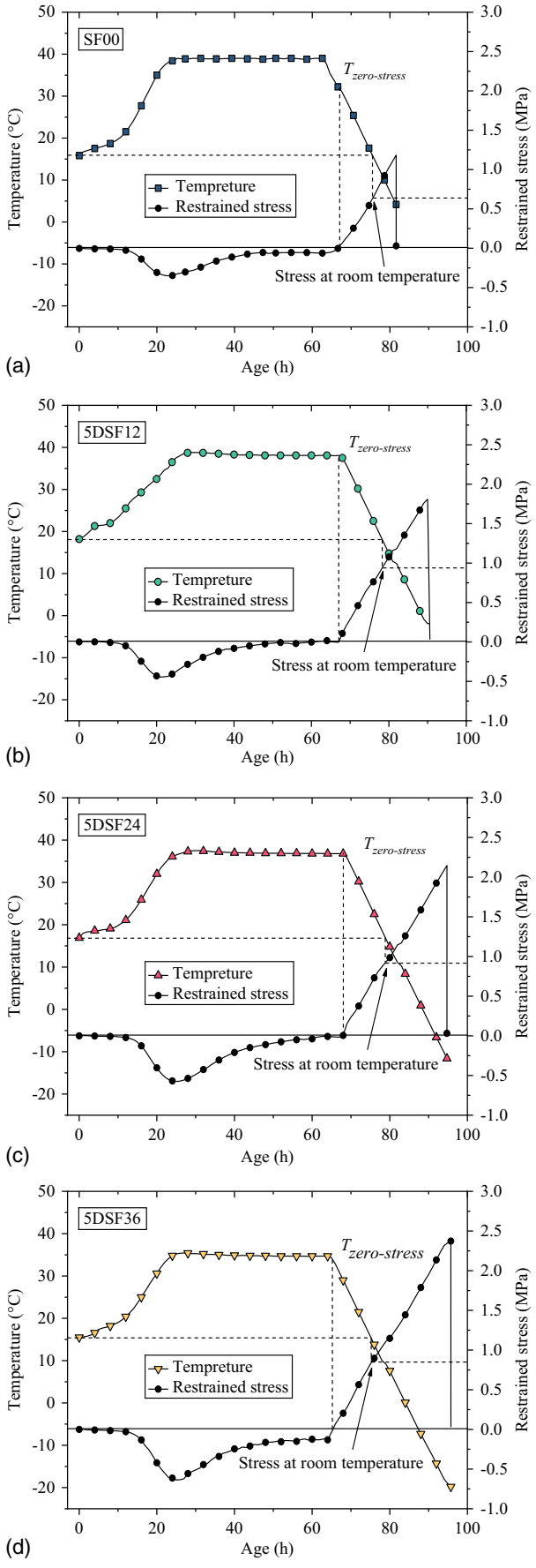

Fig. 10. Relationship between temperature or restrained stress and age of four concrete mixtures: (a) SF00; (b) 5DSF12; (c) 5DSF24; and (d) 5DSF36.

Effect of 5D Hooked-End Steel Fiber on Cracking Risk

Several factors are known to influence the cracking risk of HSC, such as humidity, temperature, and restraint degree. Many single criteria and comprehensive criteria, such as cracking stress, cracking age, ratio of cracking stress to axial tensile strength, stress reserve, and integrated criterion, have been adopted to assess the cracking risk of concrete, as recommended by Xin et al. (2020). Hence, to better assess the early-age cracking risk of 5DSFRC, some single criteria and integrated criteria were used in the present study. The results of the criteria for evaluating cracking risk of concrete are depicted in Table 5.

Ratio of Cracking Stress to Axial Tensile Strength

Generally, concrete fails when the tensile stress exceeds its tensile strength. However, the strength criteria exhibit limitations for evaluating thermal cracking. The failure stress caused by the temperature and restraint is lower than the direct or splitting tensile strength at the same age. Some premature failures are found even when the tensile stress approaches 0.50 of the direct tensile strength (Shen et al. 2018b), hence the ratio of cracking stress to axial tensile strength was used to assess the damage degree and cracking risk of 5DSFRC at early age, as reported by Shen et al. (2019b).

The actual ages of four concrete specimens were converted to the equivalent age at 20°C with Eq. (3) to determine the ratio of restrained stress to axial tensile strength at the same age, as reported by Krauß et al. (2001). The equivalent cracking age was 143.9, 145.6, 146.1, and 147.1 h for mixtures SF00, 5DSF12, 5DSF24, and 5DSF36, respectively. Axial tensile strength at the equivalent cracking age was determined with Eq. (11)

$$f_t(t) = f_{t,28} \exp\{-\lambda_1[\ln(1 + (t - t_0))]^{-k_1}\} \tag{11}$$

The results of axial tensile strength have been tested by Shen et al. (2019a), as depicted in Table 6.

The results of axial tensile strength at the equivalent cracking age for mixtures SF00, 5DSF12, 5DSF24, and 5DSF36 were 2.88, 3.26, 3.69, and 3.86 MPa, respectively. The ratio of cracking stress to axial tensile strength was 0.41, 0.56, 0.58, and 0.61 for mixtures SF00, 5DSF12, 5DSF24, and 5DSF36, which increased by 36.59%, 41.46%, and 48.78% with an increase in 5DSF volume fraction ranging from 0% to 0.12%, 0.24%, and 0.36%, respectively. The results are consistent with data obtained by Shen et al. (2019c), and the results revealed that ratio of cracking stress to the axial tensile strength of the concrete increased by 41.46% as the steel fiber volume fraction increased from 0% to 0.3%. Results indicated that the incorporation of 5DSF reduced the number of microcracks and decreased the cracking risk of concrete. Concrete is heterogeneous, and the local bearing capacity of concrete is not equal (Qi and Zhang 2008). Microcracks tend to occur in the area where tensile strength is low. The strength of concrete can be improved by adding 5DSF with a higher elastic modulus than that of the matrix (Ding and Kusterle 2000), which reduces the number of microcracks in the concrete.

Table 5. Results of criteria on evaluating cracking risk of concrete

Item	Unit	SF00	5DSF12	5DSF24	5DSF36
Cracking age	h	81.6	90.6	94.7	95.7
Cracking stress	MPa	1.18	1.81	2.15	2.37
Ratio of cracking stress to axial tensile strength	—	0.41	0.56	0.58	0.61
Stress reserve	—	0.74	0.93	1.34	1.86
Integrated criterion of cracking risk	MPa/day^2	2.08	1.96	1.67	1.53

Table 6. Axial tensile strength and regression coefficients for four mixtures

Concrete mixtures	Axial tensile strength (MPa)				
	3 d	7 d	28 d	λ_1	k_1
SF00	2.65	2.90	3.03	0.366	3.058
5DSF12	2.98	3.27	3.51	0.388	2.531
5DSF24	3.47	3.70	3.86	0.260	2.699
5DSF36	3.71	3.85	4.02	0.169	2.200

Source: Data from Shen et al. (2019a).

Stress Reserve

The stress reserve takes the stress at room temperature and cracking stress into consideration, as given in Eq. (12) (Shi et al. 2014)

$$\varphi = \frac{(\sigma_{cr} - \sigma_{rt})}{\sigma_{rt}} \times 100\% \tag{12}$$

where φ is the stress reserve; σ_{cr} is the cracking stress; and σ_{rt} is the stress at room temperature.

The results of stress reserve were 0.74, 0.93, 1.34, and 1.86 for mixtures SF00, 5DSF12, 5DSF24, and 5DSF36, which increased by 25.68%, 81.08%, and 151.35% with an increase in 5DSF volume fraction ranging from 0% to 0.12%, 0.24%, and 0.36%, respectively, as depicted in Fig. 11. Higher stress reserve indicates higher reserve strength and lower cracking risk, and results of stress reserve reveal that the incorporation of 5DSF decreases the cracking risk of HSC (Shen et al. 2016).

Integrated Criterion of Cracking Risk

Net age of cracking as well as tensile stress rate at cracking age is proposed by ASTM C1581 (ASTM 2018) to investigate cracking risk, and a modified integrated criterion of cracking risk was proposed to assess the cracking risk of 5DSFRC, as given in Eq. (13) (Shen et al. 2019c, 2021)

$$\varphi_N = \frac{S}{t_{tcr}} \tag{13}$$

where φ_N is a modified integrated criterion of cracking risk, in MPa/day^2; S is the tensile stress rate, in MPa/d; and t_{tcr} is the net age of cracking from starting point of the stage in tension to cracking age, in days.

The results of restrained tensile stress rate and net age of cracking were 1.65, 1.81, 1.87, and 1.93 MPa per day, and 19.0,

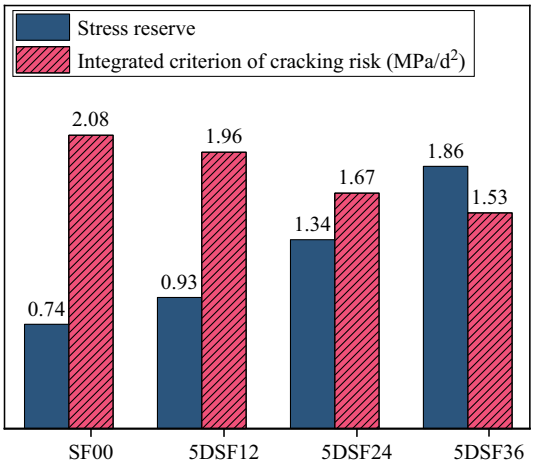

Fig. 11. Integrated criteria and stress reserve of four mixtures.

22.2, 26.8, and 30.2 h for mixtures SF00, 5DSF12, 5DSF24, and 5DSF36, respectively. The integrated criterion of cracking risk was 2.08, 1.96, 1.67, and 1.53 MPa per day^2 for mixtures SF00, 5DSF12, 5DSF24, and 5DSF36, which decreased by 5.77%, 19.71%, and 26.44% with an increase in 5DSF volume fraction ranging from 0% to 0.12%, 0.24%, and 0.36%, respectively, as depicted in Fig. 11. The results of integrated criterion φ_N indicated that the incorporation of 5DSF decreased the cracking risk of HSC. The results are consistent with data obtained by Altun et al. (2007) and Shen et al. (2019c). Shen et al. (2019c) revealed that the integrated criterion of cracking risk decreased by 11.06% when the 3DSF volume fraction increased from 0% to 0.3%. The integrated criterion of cracking risk decreased by 26.44% with an increase in 5DSF volume fraction from 0% to 0.36%. Considering that the reference concrete without steel fiber in the present study was similar to that obtained by Shen et al. (2019c), results revealed that the cracking risk of 5DSFRC was lower than that of HSC reinforced with similar volume fractions of 3DSF at early age.

Conclusion

In the present study, an investigation on temperature evolution, AS, and restrained stress was conducted to assess the cracking risk of early-age HSC reinforced with 5DSF utilizing TSTM. Based on the experiment findings, the following conclusions are obtained:

1. The AS of HSC decreased with an increase in 5DSF volume fraction. Hooked-end steel fiber showed the greatest reduction in early-age AS compared to other steel fibers of different shapes when the steel fiber volume fraction was similar. An AS formula was proposed to calculate the early-age AS of SFRC considering the effect of volume fraction and shape of steel fiber.
2. The cracking risk decreased with an increase in 5DSF volume fraction. The integrated criterion of cracking risk decreased with an increase in 5DSF volume fraction. The cracking age, cracking stress, ratio of cracking stress to axial tensile strength, and reserve strength of HSC increased with an increase in 5DSF volume fraction. The early-age cracking risk and AS of 5DSFRC were lower than that of HSC reinforced with a similar volume fraction of 3DSF.

Data Availability Statement

All data, models, and code generated or used during the study appear in the published paper.

Acknowledgments

The financial support of the National Natural Science Foundation of China (Grant No. 51879092), the Postgraduate Research & Practice Innovation Program of Jiangsu Province (Grant No. KYCX22_0614), and the support of the Fundamental Research Funds for the Central Universities (Grant No. 2019B52814) is gratefully acknowledged. This work is also supported by Science and Technology Planning Project of Jiangsu Province (Grant No. BE2022605).

References

Abdallah, S., M. Fan, and D. W. Rees. 2016. "Analysis and modelling of mechanical anchorage of 4D/5D hooked end steel fibres." *Mater. Des.* 112 (Dec): 539–552. https://doi.org/10.1016/j.matdes.2016.09.107.

Abdallah, S., M. Z. Fan, and X. M. Zhou. 2017. "Pull-out behaviour of hooked end steel fibres embedded in ultra-high performance mortar with various w/b ratios." *Int. J. Concr. Struct. Mater.* 11 (2): 301–313. https://doi.org/10.1007/s40069-017-0193-8.

Abdallah, S., D. W. A. Rees, S. H. Ghaffar, and M. Fan. 2018. "Understanding the effects of hooked-end steel fibre geometry on the uniaxial tensile behaviour of self-compacting concrete." *Constr. Build. Mater.* 178 (Jul): 484–494. https://doi.org/10.1016/j.conbuildmat.2018.05.191.

Afroughsabet, V., L. Biolzi, and T. Ozbakkaloglu. 2016. "High-performance fiber-reinforced concrete: A review." *J. Mater. Sci.* 51 (14): 6517–6551. https://doi.org/10.1007/s10853-016-9917-4.

Afroughsabet, V., L. Biolzi, and T. Ozbakkaloglu. 2017. "Influence of double hooked-end steel fibers and slag on mechanical and durability properties of high performance recycled aggregate concrete." *Compos. Struct.* 181 (Dec): 273–284. https://doi.org/10.1016/j.compstruct.2017.08.086.

Al-Naimi, H. K., and A. A. Abbas. 2021. "Shrinkage of steel-fibre-reinforced lightweight concrete." In Vol. 30 of *Proc., Fibre Reinforced Concrete: Improvements and Innovations*, edited by P. Serna, A. Llano-Torre, J. R. Martí-Vargas, and J. Navarro-Gregori, 359–367. Cham, Switzerland: Springer. https://doi.org/10.1007/978-3-030-58482-5_33.

Altun, F., T. Haktanir, and K. Ari. 2007. "Effects of steel fiber addition on mechanical properties of concrete and RC beams." *Constr. Build. Mater.* 21 (3): 654–661. https://doi.org/10.1016/j.conbuildmat.2005.12.006.

Aly, T., and J. G. Sanjayan. 2008. "Mechanism of early age shrinkage of concretes." *Mater. Struct.* 42 (4): 461–468. https://doi.org/10.1617/s11527-008-9394-6.

ASTM. 2018. *Standard test method for determining age at cracking and induced tensile stress characteristics of mortar and concrete under restrained shrinkage*. ASTM C1581/C1581M-18a. West Conshohocken, PA: ASTM.

ASTM. 2020. *Standard specification for portland cement*. ASTM C150/C150M-20. West Conshohocken, PA: ASTM.

Bandelj, B., D. Saje, J. Šušteršič, J. Lopatič, and F. Saje. 2011. "Free shrinkage of high performance steel fiber reinforced concrete." *J. Test. Eval.* 39 (2): 166–176. https://doi.org/10.1520/JTE103028.

Chen, M., H. Zhong, and M. Z. Zhang. 2020. "Flexural fatigue behaviour of recycled tyre polymer fibre reinforced concrete." *Cem. Concr. Compos.* 105 (Jan): 103441. https://doi.org/10.1016/j.cemconcomp.2019.103441.

Chinese Standard. 2018. *Common Portland cement*. [In Chinese.] Chinese Standard GB 175-2007/XG1-2018. Beijing: Standard Press of China.

Chu, I., S. H. Kwon, M. N. Amin, and J.-K. Kim. 2012. "Estimation of temperature effects on autogenous shrinkage of concrete by a new prediction model." *Constr. Build. Mater.* 35 (Oct): 171–182. https://doi.org/10.1016/j.conbuildmat.2012.03.005.

Dehghani, A., and F. Aslani. 2021. "Effect of 3D, 4D, and 5D hooked-end type and loading rate on the pull-out performance of shape memory alloy fibres embedded in cementitious composites." *Constr. Build. Mater.* 273 (Mar): 121742. https://doi.org/10.1016/j.conbuildmat.2020.121742.

De la Varga, I., J. Castro, D. Bentz, and J. Weiss. 2012. "Application of internal curing for mixtures containing high volumes of fly ash." *Cem. Concr. Compos.* 34 (9): 1001–1008. https://doi.org/10.1016/j.cemconcomp.2012.06.008.

De Smedt, M. 2018. "Monotonic and cyclic pull-out behaviour of 3D and 5D hooked-end steel fibres from a concrete matrix." In *Proc., 12th fib Int. Ph.D. Symp. in Civil Engineering*, 43–50. Lausanne, Switzerland: fib.

De Smedt, M., R. Vrijdaghs, C. Van Steen, E. Verstrynge, and L. Vandewalle. 2020. "Damage analysis in steel fibre reinforced concrete under monotonic and cyclic bending by means of acoustic emission monitoring." *Cem. Concr. Compos.* 114 (Nov): 103765. https://doi.org/10.1016/j.cemconcomp.2020.103765.

Ding, Y. N., and W. Kusterle. 2000. "Compressive stress–strain relationship of steel fibre-reinforced concrete at early age." *Cem. Concr. Res.* 30 (10): 1573–1579. https://doi.org/10.1016/S0008-8846(00)00348-3.

Døssland, Å. L. 2008. "Fibre reinforcement in load carrying concrete structures." Ph.D. thesis, Dept. of Structural Engineering, Norwegian Univ. of Science and Technology.

Gholampour, A., and T. Ozbakkaloglu. 2018. "Fiber-reinforced concrete containing ultra high-strength micro steel fibers under active confinement." *Constr. Build. Mater.* 187 (Oct): 299–306. https://doi.org/10.1016/j.conbuildmat.2018.07.042.

Guzlena, S., and G. Sakale. 2021. "Self-healing of glass fibre reinforced concrete (GRC) and polymer glass fibre reinforced concrete (PGRC) using crystalline admixtures." *Constr. Build. Mater.* 267 (Jan): 120963. https://doi.org/10.1016/j.conbuildmat.2020.120963.

Huang, H., and G. Ye. 2017. "Examining the 'time-zero' of autogenous shrinkage in high/ultra-high performance cement pastes." *Cem. Concr. Res.* 97 (Jul): 107–114. https://doi.org/10.1016/j.cemconres.2017.03.010.

Igarashi, S., A. Bentur, and K. Kovler. 2000. "Autogenous shrinkage and induced restraining stresses in high-strength concretes." *Cem. Concr. Res.* 30 (11): 1701–1707. https://doi.org/10.1016/S0008-8846(00)00399-9.

Kalpana, M., and A. Tayu. 2020. "Light weight steel fibre reinforced concrete: A review." *Mater. Today: Proc.* 22 (Jan): 884–886. https://doi.org/10.1016/j.matpr.2019.11.095.

Kang, J. C., D. J. Shen, C. C. Li, M. Li, X. D. Wang, and H. J. Hu. 2022. "Effect of water-to-cement ratio on internal relative humidity and autogenous shrinkage of early-age concrete internally cured by superabsorbent polymers." *Struct. Concr.* 23 (5): 3234–3248. https://doi.org/10.1002/suco.202100488.

Kolver, K., S. Igarashi, and A. Bentur. 1999. "Tensile creep behavior of high strength concretes at early ages." *Mater. Struct.* 32 (5): 383–387. https://doi.org/10.1007/BF02479631.

Kovler, K. 1994. "Testing system for determining the mechanical behaviour of early age concrete under restrained and free uniaxial shrinkage." *Mater. Struct.* 27 (6): 324–330. https://doi.org/10.1007/BF02473424.

Krauß, M., F. S. Rostásy, and A. W. Gutsch. 2001. *Modelling of degree of hydration on basis of adiabatic heat release*. IPACS Rep. No. BE96-3843. Luleå, Sweden: Univ. of Technology, Dept. of Civil & Mining Engineering, Div. of Structural Engineering.

Lee, S. J., D. Y. Yoo, and D. Y. Moon. 2019. "Effects of hooked-end steel fiber geometry and volume fraction on the flexural behavior of concrete pedestrian decks." *Appl. Sci.* 9 (6): 1241–1261. https://doi.org/10.3390/app9061241.

Li, H., X. Hao, Y. Liu, and Q. Wang. 2021. "Thermal effects of steel-fibre-reinforced reactive powder concrete at elevated temperatures." *Mag. Concr. Res.* 73 (3): 109–120. https://doi.org/10.1680/jmacr.19.00105.

Li, M., D. J. Shen, Q. Yang, X. Y. Cao, C. Liu, and J. C. Kang. 2022. "Rehabilitation of seismic-damaged reinforced concrete beam-column joints with different corrosion rates using basalt fiber-reinforced polymer sheets." *Compos. Struct.* 289 (Jun): 115397. https://doi.org/10.1016/j.compstruct.2022.115397.

Liu, R., H. Xiao, J. Geng, J. Du, and M. Liu. 2020. "Effect of nano-$CaCO_3$ and nano-SiO_2 on improving the properties of carbon fibre-reinforced concrete and their pore-structure models." *Constr. Build. Mater.* 244 (May): 118297. https://doi.org/10.1016/j.conbuildmat.2020.118297.

Lura, P., K. Van Breugel, and I. Maruyama. 2001. "Effect of curing temperature and type of cement on early-age shrinkage of high-performance concrete." *Cem. Concr. Res.* 31 (12): 1867–1872. https://doi.org/10.1016/S0008-8846(01)00601-9.

Maruyama, I., and P. Lura. 2019. "Properties of early-age concrete relevant to cracking in massive concrete." *Cem. Concr. Res.* 123 (Sep): 105770. https://doi.org/10.1016/j.cemconres.2019.05.015.

Meddah, M. S., P. C. Aïtcin, and N. Petrov. 2006. "A new approach for the determination of the starting point of autogenous shrinkage strains (ASS)." *Spec. Publ.* 234 (Mar): 473–484.

Meddah, M. S., and A. Tagnit-Hamou. 2011. "Evaluation of rate of deformation for early-age concrete shrinkage analysis and time zero determination." *J. Mater. Civ. Eng.* 23 (7): 1076–1086. https://doi.org/10.1061/(ASCE)MT.1943-5533.0000261.

Mehta, P. K., and P. J. M. Monteiro. 2006. *Concrete: Microstructure, properties, and materials*. 3rd ed. New York: McGraw-Hill.

Meng, W., and K. H. Khayat. 2018. "Effect of hybrid fibers on fresh properties, mechanical properties, and autogenous shrinkage of cost-effective UHPC." *J. Mater. Civ. Eng.* 30 (4): 04018030. https://doi.org/10.1061/(ASCE)MT.1943-5533.0002212.

Miao, C. W., Q. Tian, J. P. Liu, and W. Sun. 2007. "Very early age self-desiccation effect measurement based on meniscus depression technology for concrete." [In Chinese.] *J. Chin. Ceram. Soc.* 35 (4): 509–516.

Murugan, K., S. J. Stephen, and R. Gettu. 2020. "Influence of fibre geometry on the fracture of steel fibre reinforced concrete." *IOP Conf. Ser.: Mater. Sci. Eng.* 936 (1): 012025. https://doi.org/10.1088/1757-899X/936/1/012025.

Nataraja, M., N. Dhang, and A. Gupta. 1999. "Stress–strain curves for steel-fiber reinforced concrete under compression." *Cem. Concr. Compos.* 21 (5–6): 383–390. https://doi.org/10.1016/S0958-9465(99)00021-9.

Nili, M., and V. Afroughsabet. 2012. "The long-term compressive strength and durability properties of silica fume fiber-reinforced concrete." *Mater. Sci. Eng., A* 531 (Jan): 107–111. https://doi.org/10.1016/j.msea.2011.10.042.

Pająk, M., and T. Ponikiewski. 2013. "Flexural behavior of self-compacting concrete reinforced with different types of steel fibers." *Constr. Build. Mater.* 47 (Oct): 397–408. https://doi.org/10.1016/j.conbuildmat.2013.05.072.

Qi, F., and W. J. Zhang. 2008. "Fiber concrete under temperature drop load with stochastic FEM." *J. Shanghai Jiaotong Univ.* 13 (2): 161–165. https://doi.org/10.1007/s12204-008-0161-1.

Şahmaran, M., M. Al-Emam, G. Yıldırım, Y. E. Şimşek, T. K. Erdem, and M. Lachemi. 2013. "High-early-strength ductile cementitious composites with characteristics of low early-age shrinkage for repair of infrastructures." *Mater. Struct.* 48 (5): 1389–1403. https://doi.org/10.1617/s11527-013-0241-z.

Şahmaran, M., M. Lachemi, K. M. A. Hossain, and V. C. Li. 2009. "Internal curing of engineered cementitious composites for prevention of early age autogenous shrinkage cracking." *Cem. Concr. Res.* 39 (10): 893–901. https://doi.org/10.1016/j.cemconres.2009.07.006.

Saje, D., B. Bandelj, J. Šušteršic, J. Lopatic, and F. Saje. 2012. "Autogenous and drying shrinkage of fibre reinforced high-performance concrete." *J. Adv. Concr. Technol.* 10 (2): 59–73. https://doi.org/10.3151/jact.10.59.

Schlitter, J., D. P. Bentz, and W. J. Weiss. 2013. "Quantifying stress development and remaining stress capacity in restrained, internally cured mortars." *ACI Mater. J.* 110 (1): 3–11.

Shah, H. R., and J. Weiss. 2006. "Quantifying shrinkage cracking in fiber reinforced concrete using the ring test." *Mater. Struct.* 39 (9): 887–899. https://doi.org/10.1617/s11527-006-9089-9.

Shen, D. J., J. L. Jiang, J. X. Shen, P. P. Yao, and G. Q. Jiang. 2016. "Influence of curing temperature on autogenous shrinkage and cracking resistance of high-performance concrete at an early age." *Constr. Build. Mater.* 103 (Jan): 67–76. https://doi.org/10.1016/j.conbuildmat.2015.11.039.

Shen, D. J., J. L. Jiang, W. T. Wang, J. X. Shen, and G. Q. Jiang. 2017. "Tensile creep and cracking resistance of concrete with different water-to-cement ratios at early age." *Constr. Build. Mater.* 146 (Aug): 410–418. https://doi.org/10.1016/j.conbuildmat.2017.04.056.

Shen, D. J., J. L. Jiang, M. Y. Zhang, P. P. Yao, and G. Q. Jiang. 2018a. "Tensile creep and cracking potential of high performance concrete internally cured with super absorbent polymers at early age." *Constr. Build. Mater.* 165 (Mar): 451–461. https://doi.org/10.1016/j.conbuildmat.2017.12.136.

Shen, D. J., J. C. Kang, Y. Jiao, M. Li, and C. C. Li. 2020. "Effects of different silica fume dosages on early-age behavior and cracking resistance of high strength concrete under restrained condition." *Constr. Build. Mater.* 263 (Dec): 120218. https://doi.org/10.1016/j.conbuildmat.2020.120218.

Shen, D. J., J. C. Kang, C. Liu, M. Li, Y. F. Wei, and L. K. Zhou. 2022a. "Effect of temperature rise inhibitor on early-age behavior and cracking resistance of high strength concrete under uniaxial restrained condition." *J. Build. Eng.* 45 (Apr): 103496. https://doi.org/10.1016/j.jobe.2021.103496.

Shen, D. J., J. C. Kang, X. J. Yi, L. K. Zhou, and X. Shi. 2019a. "Effect of double hooked-end steel fiber on early-age cracking potential of high strength concrete in restrained ring specimens." *Constr. Build. Mater.* 223 (Oct): 1095–1105. https://doi.org/10.1016/j.conbuildmat.2019.07.319.

Shen, D. J., C. Liu, J. C. Kang, Q. Yang, M. Li, C. C. Li, and X. Zeng. 2022b. "Early-age autogenous shrinkage and tensile creep of hooked-end steel fiber reinforced concrete with different thermal treatment temperatures." *Cem. Concr. Compos.* 131 (Aug): 104550. https://doi.org/10.1016/j.cemconcomp.2022.104550.

Shen, D. J., C. Liu, C. C. Li, X. G. Zhao, and G. Q. Jiang. 2019b. "Influence of Barchip fiber length on early-age behavior and cracking resistance of concrete internally cured with super absorbent polymers." *Constr. Build. Mater.* 214 (Jul): 219–231. https://doi.org/10.1016/j.conbuildmat.2019.03.209.

Shen, D. J., C. Liu, M. Wang, J. C. Kang, and M. Li. 2021. "Effect of polyvinyl alcohol fiber on the cracking risk of high strength concrete under uniaxial restrained condition at early age." *Constr. Build. Mater.* 300 (Sep): 124206. https://doi.org/10.1016/j.conbuildmat.2021.124206.

Shen, D. J., X. Z. Liu, Q. Y. Li, L. Sun, and W. T. Wang. 2019c. "Early-age behavior and cracking resistance of high-strength concrete reinforced with Dramix 3D steel fiber." *Constr. Build. Mater.* 196 (Jan): 307–316. https://doi.org/10.1016/j.conbuildmat.2018.10.125.

Shen, D. J., W. T. Wang, J. W. Liu, X. G. Zhao, and G. Q. Jiang. 2018b. "Influence of Barchip fiber on early-age cracking potential of high performance concrete under restrained condition." *Constr. Build. Mater.* 187 (Oct): 118–130. https://doi.org/10.1016/j.conbuildmat.2018.07.121.

Shen, D. J., X. Wang, and S. X. Wu. 2022c. "Determining hydration mechanisms for initial fall and main hydration peak in tricalcium silicate hydration using a two-scale hydration simulation model." *Cem. Concr. Res.* 156 (Jun): 106763. https://doi.org/10.1016/j.cemconres.2022.106763.

Shi, N. N., J. S. Ouyang, R. X. Zhang, and D. H. Huang. 2014. "Experimental study on early-age crack of mass concrete under the controlled temperature history." *Adv. Mater. Sci. Eng.* 12 (3): 352–358. https://doi.org/10.1155/2014/671795.

Sun, W., A. M. James, and S. Samir. 1986. "Study of the interface strength in steel fiber-reinforced cement-based composites." *ACI J. Proc.* 83 (4): 597–605. https://doi.org/10.14359/10453.

Tang, S. W., D. S. Huang, and Z. He. 2021. "A review of autogenous shrinkage models of concrete." *J. Build. Eng.* 44 (Dec): 103412. https://doi.org/10.1016/j.jobe.2021.103412.

Tazawa, E., and S. Miyazawa. 1995. "Influence of cement and admixture on autogenous shrinkage of cement paste." *Cem. Concr. Res.* 25 (2): 281–287. https://doi.org/10.1016/0008-8846(95)00010-0.

Tenório Filho, J. R., M. A. Pereira Gomes de Araújo, D. Snoeck, and N. De Belie. 2019. "Discussing different approaches for the time-zero as start for autogenous shrinkage in cement pastes containing superabsorbent polymers." *Materials* 12 (18): 2962–2977. https://doi.org/10.3390/ma12182962.

Turcry, P., A. Loukili, L. Barcelo, and J. M. Casabonne. 2002. "Can the maturity concept be used to separate the autogenous shrinkage and thermal deformation of a cement paste at early age?" *Cem. Concr. Res.* 32 (9): 1443–1450. https://doi.org/10.1016/S0008-8846(02)00800-1.

Venkateshwaran, A., K. H. Tan, and Y. Li. 2018. "Residual flexural strengths of steel fiber reinforced concrete with multiple hooked-end fibers." *Struct. Concr.* 19 (2): 352–365. https://doi.org/10.1002/suco.201700030.

Viviani, M., B. Glisic, and I. Smith. 2007. "Separation of thermal and autogenous deformation at varying temperatures using optical fiber sensors." *Cem. Concr. Compos.* 29 (6): 435–447. https://doi.org/10.1016/j.cemconcomp.2007.01.005.

Voigt, T., G. Ye, Z. Sun, S. P. Shah, and K. van Breugel. 2005. "Early age microstructure of Portland cement mortar investigated by ultrasonic shear waves and numerical simulation." *Cem. Concr. Res.* 35 (5): 858–866. https://doi.org/10.1016/j.cemconres.2004.09.004.

Wei, Y., and W. Hansen. 2013. "Tensile creep behavior of concrete subject to constant restraint at very early ages." *J. Mater. Civ. Eng.* 25 (9): 1277–1284. https://doi.org/10.1061/(ASCE)MT.1943-5533.0000671.

Weiss, W. J., W. Yang, and S. P. Shah. 1998. "Shrinkage cracking of restrained concrete slabs." *J. Eng. Mech.* 124 (7): 765–774. https://doi.org/10.1061/(ASCE)0733-9399(1998)124:7(765).

Wu, L. M., N. Farzadnia, C. J. Shi, Z. H. Zhang, and H. Wang. 2017. "Autogenous shrinkage of high performance concrete: A review." *Constr. Build. Mater.* 149 (Sep): 62–75. https://doi.org/10.1016/j.conbuildmat.2017.05.064.

Xin, J. D., G. X. Zhang, Y. Liu, Z. H. Wang, and Z. Wu. 2020. "Evaluation of behavior and cracking potential of early-age cementitious systems using uniaxial restraint tests: A review." *Constr. Build. Mater.* 231 (Jan): 117146. https://doi.org/10.1016/j.conbuildmat.2019.117146.

Zhang, J., H. D. Wei, and S. Wei. 2010. "Experimental study on the relationship between shrinkage and interior humidity of concrete at early age." *Mag. Concr. Res.* 62 (3): 191–199. https://doi.org/10.1680/macr.2010.62.3.191.

Zhang, T., and W. Z. Qin. 2006. "Tensile creep due to restraining stresses in high-strength concrete at early ages." *Cem. Concr. Res.* 36 (3): 584–591. https://doi.org/10.1016/j.cemconres.2005.11.017.

Zhao, Z. F., K. J. Wang, D. A. Lange, H. G. Zhou, W. L. Wang, and D. M. Zhu. 2019. "Creep and thermal cracking of ultra-high volume fly ash mass concrete at early age." *Cem. Concr. Compos.* 99 (May): 191–202. https://doi.org/10.1016/j.cemconcomp.2019.02.018.

Zheng, X. Y., T. Ji, S. M. Easa, B. B. Zhang, and Z. L. Jiang. 2019. "Tensile basic creep behavior of lightweight aggregate concrete reinforced with steel fiber." *Constr. Build. Mater.* 200 (Mar): 356–367. https://doi.org/10.1016/j.conbuildmat.2018.12.138.

Zhu, J., D. J. Shen, B. S. Jin, and S. X. Wu. 2022a. "Theoretical investigation on the formation mechanism of carbonate ion in microbial self-healing concrete: Combined QC calculation and MD simulation." *Constr. Build. Mater.* 342 (Aug): 128000. https://doi.org/10.1016/j.conbuildmat.2022.128000.

Zhu, J., D. J. Shen, J. J. Xie, B. S. Jin, and S. X. Wu. 2022b. "Transformation mechanism of carbamic acid elimination and hydrolysis reaction in microbial self-healing concrete." *Mol. Simul.* 48 (8): 719–735. https://doi.org/10.1080/08927022.2022.2049773.